Molecular Dynamics Simulations of Electroosmosis in Perfluorosulfonic Acid Polymer

ARTICLE *in* THE JOURNAL OF PHYSICAL CHEMISTRY B · JUNE 2008

Impact Factor: 3.3 · DOI: 10.1021/jp7121449 · Source: PubMed

3 AUTHORS, INCLUDING:

Liuming Yan
Shanghai University
66 PUBLICATIONS **832** CITATIONS
SEE PROFILE

Wencong Lu
Shanghai University
56 PUBLICATIONS **693** CITATIONS
SEE PROFILE

Molecular Dynamics Simulations of Electroosmosis in Perfluorosulfonic Acid Polymer

Liuming Yan,*,† Xiaobo Ji,‡,† and Wencong Lu†

Department of Chemistry, College of Sciences, and School of Material Science and Engineering, Shanghai University, 99 Shangda Road, Shanghai 200444, China

Received: December 29, 2007

An atomistic MD simulation method has been developed to study the electroosmotic drag in the hydrated perfluorosulfonic acid polymer. The transport characteristics of the hydroniums and water molecules are evaluated from their velocity distribution functions with an electric field applied. It is shown that the microstructure of the hydrated perfluorosulfonic acid polymer is not perturbed significantly by the electric field up to 2 V/μm, and the velocity distribution functions obey the peak shifted Maxwell velocity distribution functions. The evaluated peak shifting velocities are only about 1% of the average thermal motion. The hydronium flow and water flow are evaluated from the average transport velocities or the peak shifting velocities. The electroosmotic drag coefficients from the MD simulations are in good correspondence with the experimental values. It is also shown that the electroosmotic drag coefficient has no or weak temperature dependence.

1. Introduction

The proton exchange membrane fuel cell (PEMFC) is a competent candidate for application in vehicles due to its high-energy conversion efficiency, high-energy density, and environmental friendliness.[1,2] Among the many proton exchange materials, perfluorosulfonic acid (PFSA) polymers are the most preferred electrolyte materials for hydrogen fuel cells. Despite the great progress achieved in recent years, both economic and technical challenges are yet to be overcome for the large-scale commercialization of fuel cells in vehicles. The economic and technical challenges are usually interrelated. For example, the cost of the electrocatalysts could be reduced by improving their activity thus reducing the catalysts loading or by substituting with cheap electrocatalysts.[3−5] Increasing the fuel cell operation temperature could also increase the catalytic activity and the CO tolerance;[6] however, the high-temperature proton conductivity of the proton exchange membrane should be greatly improved.[6,7] Presently, the middle-temperature fuel cells (working at about 80 °C) are the most successful technology available. One of the obstacles for the middle-temperature fuel cell is the complexity of water management. On the one hand, low water content can affect the hydration of the PFSA membrane and reduce its proton conductivity.[8,9] On the other hand, surplus water content can cause cathode flooding and retard the transport of oxygen.[9−11] These factors can significantly degrade the performance of fuel cells, or even cause the operational failure of the fuel cells.[12,13]

The water management of fuel cells depends on several factors: the water evaporation speed which depends on the operational temperature, the vapor content in the fed gas, the electroosmotic drag of water, and so on.[9,10] Electroosmotic drag is the water transport accompanying proton transport through the membrane, which is evaluated by the electroosmotic drag coefficient defined as the number of water molecules transported with the transport of each proton.[14,15] Although various experimental techniques have been developed for the measurement of the electroosmotic drag coefficient, the experimental electroosmotic drag coefficient still differs from measurement to measurement due to the complexity of electroosmotic mechanism and the coupling between several of the water transport phenomena.[15] For details of the experimental methods, the readers should see refs 15−18.

The other important application fields of electroosmotic drag or similar electrophoresis are found in the analysis and separation of biomolecules,[19] in the removal of contaminants from soils, and in the dewatering of waste sludge.[20] A recent application of the electroosmotic drag is in the controlling of fluidic flow in microfluidic or nanofluidic systems.[21,22]

The electroosmotic drag has been explained by the classic mechanistic theory,[23−26] the hydrodynamic model,[27] the statistical mechanics theory,[28] the continuum model based on Navier Stokes equations,[29] the macroscopic model with incorporation of nanoscopic information,[14] and so on. These theories can qualitatively explain some of the characteristics of electroosmotic drag; however, their predictions often deviate from experimental measurements and depend on the input parameters. As an important complement to the theoretical and experimental methods, molecular dynamics (MD) simulations are also applied to the study of electroosmotic transport.[30−35] Since these simulations are based on the direct evaluation of the electric field induced average transport velocities, which are only a few percent of the overall thermal motion, statistical convergence is a great problem. To accelerate the statistical convergence, an extremely high electric field up to 100 V/μm or more has to be applied in the simulations to accelerate the molecular transport.[32,35]

In this work, we develop a new method for the evaluation of the electroosmotic drag coefficient from the average transport velocities of hydroniums and water molecules based on the molecular velocity distribution functions using MD simulations with an electric field applied. The main advantage of this method is fast convergence of the statistics, and thus, the applied electric

* To whom correspondence should be addressed. Phone: 8621-66132405. E-mail: liuming.yan@shu.edu.cn.
† Department of Chemistry, College of Sciences.
‡ School of Material Science and Engineering.

10.1021/jp7121449 CCC: $40.75
Published on Web 05/01/2008

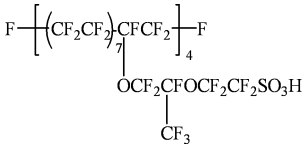

Figure 1. Molecular model of the PFSA membrane; each oligomer consists of a poly(tetrafluoroethylene) backbone and four pendant side chains terminated by a sulfonic acid group.

field could be greatly reduced to a strength that will not significantly perturb the microstructure of the system. We also studied the structural characteristics of PFSA with an electric field applied. To our knowledge, this is the first atomistic MD simulation study of the electroosmosis of hydrated PFSA membrane based on the evaluation of velocity distribution functions.

2. The Molecular Models and the Calculation Methods

2.1. The Molecular Models. The simulated system is composed of four PFSA molecules, which are modeled by oligomers each consisting of a 64-carbon long poly(tetrafluoroethylene) backbone and four pendant side chains terminated by sulfonic acid groups (Figure 1), and 320 water molecules corresponding to a hydration degree of 20. All the sulfonic acid groups are supposed to be ionized leaving a negatively charged sulfonate ion SO_3^-, and forming 16 hydroniums to keep the neutrality of the system.

The initial configuration of a simulated system is obtained by the following process: the PFSA oligomers are first added, and then hydroniums and water molecules are randomly inserted into the void space of the simulation cell. The density of the initial configuration is only about 0.5 g/cm^3. During the simulation, the simulation cell is gradually squeezed and reaches its equilibrium density.

In our simulation, the all-atom force-field models are applied to the hydrated PFSA oligomers, water molecules, and hydroniums. The total energy of the simulated system is a sum over all the intramolecular and intermolecular interactions. The intramolecular interactions include the bond stretching,

$$u_b = \sum_i \frac{1}{2} K_b (b - b_0)^2 \tag{1}$$

the bond angle bending,

$$u_\theta = \sum_i \frac{1}{2} K_\theta (\theta - \theta_0)^2 \tag{2}$$

and dihedral torsion,

$$u_\varphi = \sum_i \frac{1}{2} K_\varphi (1 + \cos 3\varphi) \tag{3}$$

The intermolecular interactions, or nonbonding interactions, are summed over all pairs of van der Waals interactions,

$$u_{LJ} = \sum_i \sum_{j<i} 4\epsilon_{ij}((\sigma_{ij}/r_{ij})^{12} - (\sigma_{ij}/r_{ij})^6) \tag{4}$$

and electrostatic interactions,

$$u_{coul} = \sum_i \sum_{j<i} \frac{q_i q_j}{4\pi\epsilon_0 r_{ij}} \tag{5}$$

The details of the all-atom force-field model for PFSA are described elsewhere.[8] The rigid TIP3P force-field model is used for the water molecules.[36,37] The modified TIP3P model is used for the hydroniums.[38]

2.2. The Simulation Details. The MD simulations are carried out by use of the DL_POLY program.[39] Lennard-Jones interactions and electrostatic potentials are cut off at 8.5 Å. The Ewald summation is applied to the calculation of electrostatic potential in account for long-range corrections. The temperature and pressure are maintained by the Nosé−Hoover thermostat with relaxation time of 0.1 ps.[40,41] The integration algorithm used is the Verlet scheme, and the integration step time is 1 fs.[42]

During the simulation, 1 000 000 time steps are run in the first period to ensure that the system reaches equilibrium. And then 2 000 000 production steps are carried out and snapshots of the coordinates and velocities of all atoms are recorded every 100 time steps in the history files. The recorded history files are used to generate the various properties.

In the case that an electric field is applied, the simulations are started from the same initial configuration as the one without an electric field applied; however, the simulation processes are slightly different. In the first period, 1 000 000 time steps are run to ensure that the system reaches equilibrium. Then, the electric fields are turned on and 300 000 more time steps are run before the production run. Finally, 2 000 000 production steps are run with the electric field still applied. The other processes are the same as the one without an electric field applied.

2.3. The Evaluation of the Velocity Distribution Functions. The speed or velocity distribution functions are evaluated by using the history files recorded during the production run. And then, these distribution functions are fitted to the Maxwell speed distribution function,

$$f(v) = 4\pi v^2 (m/2\pi kT)^{3/2} \exp(-mv^2/2kT) \tag{6}$$

or the Maxwell velocity distribution function in directions perpendicular to the applied electric field,

$$f(v_\perp) = \sqrt{m/2\pi kT_\perp}\, \exp(-mv_\perp{}^2/2kT_\perp) \tag{7}$$

or the peak shifted Maxwell velocity distribution function in the direction of the applied electric field,

$$f(v_{||}) = \sqrt{m/2\pi kT_{||}} \exp(-m(v_{||} - v_0)^2/2kT_{||}) \tag{8}$$

From these nonlinear fits, we get three different types of temperatures for hydronium (water), the overall temperature T_h (T_w), the temperature in directions perpendicular to the electric field $T_{h,\perp}$ ($T_{w,\perp}$), and the temperature in the direction of the electric field $T_{h,||}$ ($T_{w,||}$). We also get the peak shifting velocity $v_{0,h}$ ($v_{0,w}$) for hydronium (water) induced by the electric field.

2.4. The Evaluation of Average Transport Velocities and Electroosmotic Drag Coefficient. The electroosmotic drag coefficient, K_{drag}, is defined as the number of water molecules transported accompanied by the transport of each proton.[14,15] Therefore, it could be calculated as,

$$K_{drag} = \frac{J_w + J_h(veh)}{J_h(veh)} \tag{9}$$

where J_h(veh) or J_w are the hydronium flow or the water flow exclusively due to the applied electric field without any other mechanism. The hydronium (water) flow could be evaluated as a multiplication of its concentration and average transport velocity induced by the electric field,

$$J_h(\text{veh}) = \frac{n_h}{V}\bar{v}_h \tag{10A}$$

$$J_w = \frac{n_w}{V}\bar{v}_w \tag{10B}$$

where V is the volume of the simulated system, n_h (n_w) is the number of hydroniums (water molecules), and $\bar{v}_h$ ($\bar{v}_w$) is the average transport velocity of hydronium (water).

Three different methods could be used to evaluate the average transport velocities. The first method is the direct method, which evaluates the average transport velocities by summation of the velocities $v_h(i,\tau)$ (or $v_w(i,\tau)$) at all time steps τ and over all hydroniums (or water molecules),

$$\bar{v}_h = \frac{1}{m}\sum_{\tau=1}^{m}\frac{1}{n_h}\sum_{i=1}^{n_h} v_h(i,\tau) \tag{11A}$$

$$\bar{v}_w = \frac{1}{m}\sum_{\tau=1}^{m}\frac{1}{n_w}\sum_{i=1}^{n_w} v_w(i,\tau) \tag{11B}$$

The summation is over all n_h (n_w) hydronium (water molecules) and all m time steps recorded in the history file. However, this direct method converges too slowly and undesirably high electric field has to be applied to overcome the statistical fluctuation. The second method is based on the integration of the velocity distribution functions obtained from the MD simulations,

$$\bar{v}_h = \int_{-\infty}^{\infty} f(v_{h,||})\, v_{h,||}\, \mathrm{d}v_{h,||} \tag{12A}$$

$$\bar{v}_w = \int_{-\infty}^{\infty} f(v_{w,||})\, v_{w,||}\, \mathrm{d}v_{w,||} \tag{12B}$$

In this method, the average transport velocities converge satisfactorily. In the third method, the average transport velocities are approximated by the peak shifting velocities from the best fits to the shifted Maxwell distribution functions (eq 8). If the velocity distribution functions from the MD simulations exactly obey the peak-shifted Maxwell distribution functions, the peak shifting velocities are the same as the average transport velocities from the second method. However, the velocity distribution functions from MD simulations usually do not agree exactly with the peak-shifted Maxwell velocity distribution functions especially when the applied electric field is high.

3. Results and Discussions

3.1. Microstructure of the Hydrated PFSA Membrane with an Electric Field Applied. To study the perturbation from the electric field, various electric fields of 0, 2, 5, 7, or 10 V/μm are applied in the x-direction of the simulated systems. Our simulations show that the microstructures of the hydrated PFSA are not significantly perturbed by electric field up to 2 V/μm; however, the microstructures will be greatly perturbed by the electric field at 5 V/μm or more (Figure 2).

The first significant difference is the subphase structure of the hydrated PFSA. Without or with weak electric field, the microstructures are similar to what have been reported in numerous literatures with the fluorocarbon backbones of PFSA forming hydrophobic subphase, and with the hydrophilic side chains, water molecules, and hydroniums forming hydrophilic subphase (Figure 2a,b). When a high electric field is applied, the division between the hydrophilic subphase and the hydrophobic subphase disappears, and the water molecules and hydroniums are scattered in the hydrophobic subphase (Figure 2c−e).

The second significant difference is the conformation of the PFSA oligomers. Under weak electric field, the PFSA oligomer strands still maintain irregular thread conformations. However, under strong electric field, the PFSA oligomer strands are stretched with the acidic side chains directing opposite to the electric field because of the electric field pulling on the sulfonate anion.

The third significant difference is the density of the hydrated PFSA. The stretched conformations have lower density than the irregular thread conformations since the packing of the stretched PFSA strands is looser than that of the twisted irregular strands. Supposing that the dry density of PFSA is 2.0 g/cm^3, which is the density of a typical commercial PFSA (NAFION),[43] the theoretical density of the hydrated PFSA is about 1.74 g/cm^3 by ideal mixing. From Table 1 it could be seen that the simulated density at zero electric field is 1.72 g/cm^3, close to the theoretical density. However, as the electric field increases, the density gradually decreases to 1.53 g/cm^3 at an electric field of 10 V/μm, only 87.9% of the theoretical density.

These structural characteristics could be explained by the relative strength of the electric pulling force on hydroniums and the intermolecular attraction force that maintains the hydrophilic subphase. For example, the intermolecular attraction force between two TIP3P water molecules is a summation of the Coulombic interaction and the Lennard-Jones interaction. By ignoring the Coulombic interaction, the intermolecular force between two TIP3P water molecules is,

$$F_{LJ} = -\frac{\mathrm{d}u_{LJ}}{\mathrm{d}r} = (24\epsilon/r)[2(\sigma/r)^{12} - (\sigma/r)^6] \tag{13}$$

And the maximum intermolecular attraction is,

$$F_{max} = -(504/169)\sqrt[6]{7/26}(\epsilon/\sigma) \approx -2.40(\epsilon/\sigma) \tag{14}$$

For TIP3P water, the Lennard-Jones parameters are $\sigma = 3.15$ Å and $\epsilon = 6.60$ meV. Thus the maximum Lennard-Jones attraction between two TIP3P water molecules is about 5.0 meV/Å.

When an electric field is applied to the hydrated PFSA, the hydroniums and sulfonate groups are pulled by the external electric field. The electric pulling force on a hydronium cation is $F_{pull} = qE$, where q is charge of a proton and E is the electric field. If the electric field is 2 V/μm, the electric pulling force is 0.2 meV/Å. This electric pulling force is only 4% of the maximum Lennard-Jones attractions between two TIP3P water molecules. Although the intermolecular attractions between other molecules may be smaller than the intermolecular attraction between two water molecules, this conclusion will not significantly change. Therefore, we conclude that the electric perturbation is not significant at 2 V/μm. On the other hand, if the electric field is raised to 100 V/μm, the electric pulling force on a hydronium cation will be 10 meV/Å, which is twice the maximum intermolecular attraction force between two TIP3P water molecules. This electric pulling force could overcome the intermolecular attraction and pull the hydroniums out of the hydrophilic subphase. As a result, the microstructure of the hydrated PFSA membrane will be significantly perturbed.

It is common knowledge that water molecules can evaporate at elevated temperatures without any electric pulling force because of the thermal motion. And the hydroniums will also escape the attraction of the hydrophilic subphase. Therefore, it is a reasonable deduction that the hydroniums can escape the

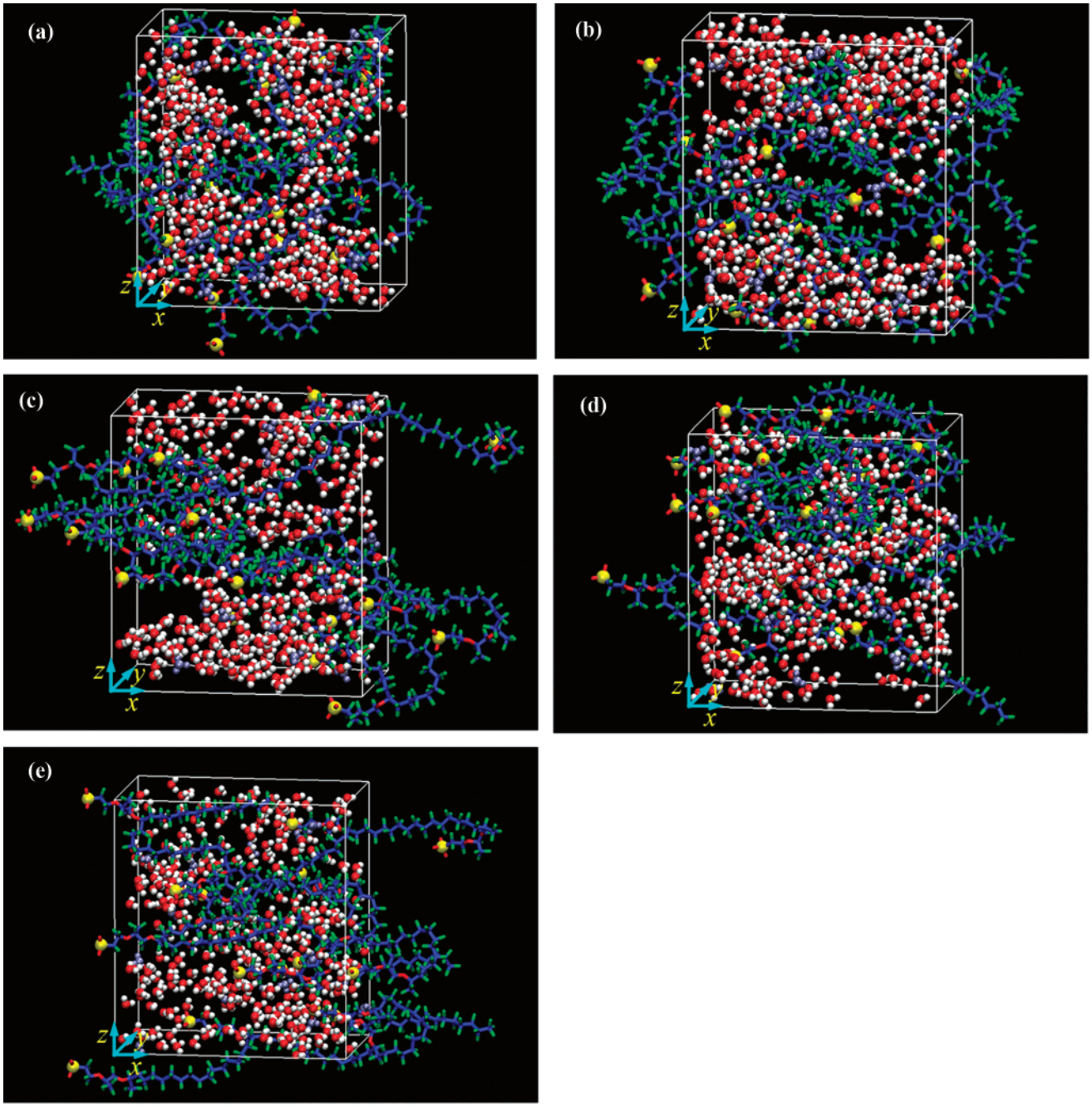

Figure 2. The snapshots of the microstructures of the hydrated PFSA with an electric field applied in the *x*-direction at (a) 0, (b) 2 , (c) 5 , (d) 7, and (e) 10 V/μm. Notice that these snapshots do not match exactly the simulation cells (the white box) since the molecules that span between two simulation cells have been adjusted to show their continuous images by applying the periodical boundary conditions. The PFSA oligomers are represented by licorice models with the sulfur atoms highlighted by the big yellow balls, the hydroniums and water molecules by the ball-and-stick models. Color code: O (red), H (white), C (blue), F (green), S (yellow), hydronium (gray). Simulation parameters: 300 K and 1 atm with NPT ensemble.

TABLE 1: The Densities and Various Temperatures of the Hydrated PFSA Simulated at 300 K, 1 atm, and with Various Electric Fields (units: *E*, V/μm; ρ, g/cm^3; *T*, K)

E	ρ	T_h	$T_{h,\|\|}$	$T_{h,\perp}$	T_w	$T_{w,\|\|}$	$T_{w,\perp}$
0	1.72	300.7	300.0	300.7	300.0	300.0	300.1
2	1.71	310.6	311.8	309.1	306.0	306.6	305.8
5	1.61	468.1	495.3	420.2	407.4	416.7	394.7
7	1.59	470.4	728.2	500.1	610.5	476.2	441.6
10	1.53	960.9	1199.7	617.6	463.1	498.9	447.6

attraction of the hydrophilic subphase at elevated temperatures even when the electric pulling force is much weaker than the intermolecular attraction force. From our simulation, it is revealed that the temperature will also increase during the MD simulations because of the accumulation of electric heat. And the microstructure of the hydrated PFSA is the combined results of the electric pulling, the thermal motion, and heat accumulation. We will discuss the heat accumulation and temperature increases of the simulated systems during the MD simulations with an electric field applied in section 3.3.

3.2. The Speed and Velocity Distribution Functions of Hydroniums and Water Molecules. The various speed distribution functions of hydroniums and water molecules with various electric fields applied are evaluated by using history files recorded during the production run. At electric fields of 0 and 2 V/μm, the speed distribution functions agree well with the Maxwell speed distribution functions (Figure 3). The

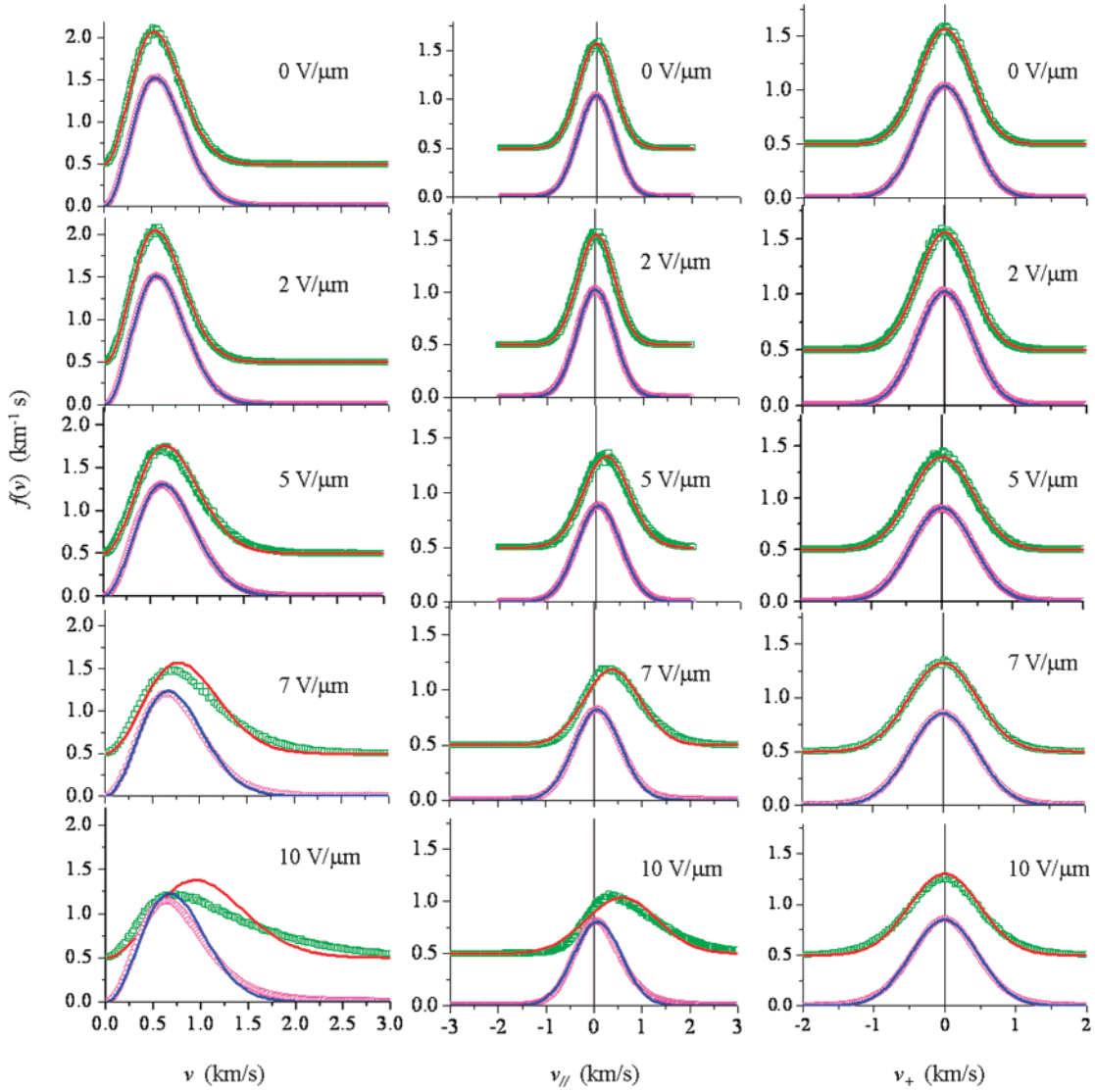

Figure 3. The various speed or velocity distribution functions of hydroniums and water molecules simulated at various electric fields and their best fits to the Maxwell distribution functions: left column, Speed distribution functions; middle column, velocity distribution function in direction of the applied electric field, and right column, velocity distribution functions in the direction perpendicular to the electric field. Green open squares (purple open circles) represent data points for the velocity distribution of hydroniums (water molecules) evaluated from MD simulations; red (blue) curves represent the best fits to the Maxwell distribution functions (or the peak shifted ones). To separate the two sets of distribution functions, the distribution functions for hydroniums have been shifted on the vertical axis. Simulation parameters: 300 K and 1 atm with NPT ensemble.

distribution functions of hydroniums and water molecules are very similar to each other except for the fact that a hydronium is slightly heavier than a water molecule, thus the hydroniums move slightly slower than the water molecules. At 5 V/μm, the speed distribution function begins to deviate from the Maxwell distribution function, and the peak height from the MD simulation is lower than the one predicted by the Maxwell distribution function. At 7 or 10 V/μm, the differences between the speed distribution functions from MD simulations and what are predicted by the Maxwell distribution functions are significant, especially for the hydroniums (Figure 3). Therefore, we conclude that the transport characteristics of the hydroniums and water molecules are greatly perturbed by the electric field.

For the velocity distribution function in the direction of the applied electric field, it agrees with the peak-shifted Maxwell distribution function (eq 8) up to 5 V/μm (Figure 3). Table 2 lists the peak shifting velocities of hydronium and water simulated with various electric fields applied. At 2 V/μm, the peak shifting velocities of hydronium and water are 21.9 and 6.7 m/s, respectively, while at 5 V/μm, the peak shifting velocities suddenly increase to 216.1 and 61.4 m/s. This is another piece of evidence that the electric pulling force on the hydronium overcomes the intermolecular attraction force, and the hydronium and water molecules escape from the hydrophilic subphase. When the applied electric field is increased to 7 or 10 V/μm, the peak shifting velocities increase more sharply (Table 2).

The velocity distribution function in the direction perpendicular to the applied electric field agrees very well with the Maxwell velocity distribution functions up to 10 V/μm (Figure 3). However, a different temperature parameter, shown in Table 1 as $T_{h,\perp}$ and $T_{w,\perp}$, has to be used to fit the velocity distribution function to the Maxwell velocity distribution function since kinetic energy is rearranged between the direction of the electric field and the directions perpendicular to the electric field during the collisions.

3.3. The Temperatures of Hydrated PFSA Simulated with an Electric Field Applied. In experiment, the applied electric field is much lower than the one used in our simulations. For example, the typical electric field in a practical polymer

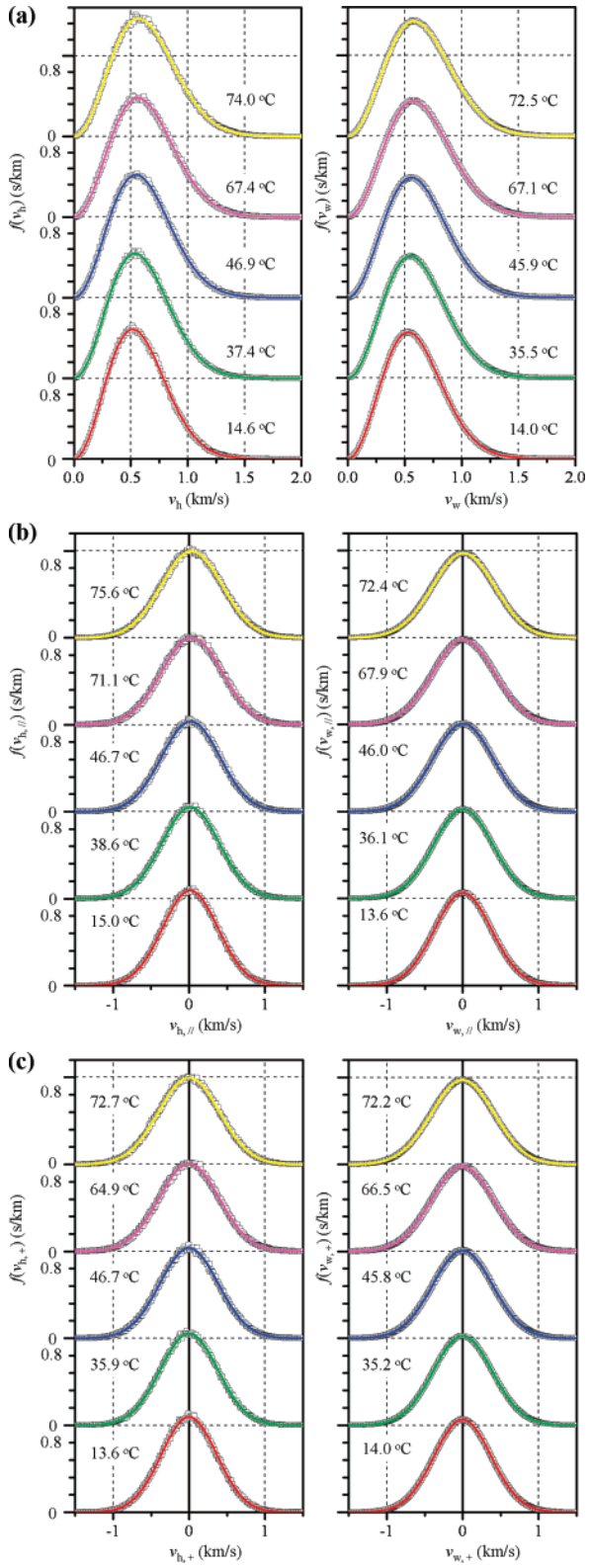

Figure 4. Various velocity distribution functions of the hydroniums and water molecules in hydrated PFSA, simulated at various temperatures with an electric field of 2 V/μm applied: (a) speed distribution functions, (b) velocity distribution in the direction of the applied electric field, and (c) velocity distribution in the direction perpendicular to the applied electric field. The left panels are for hydroniums, and the right panels are for the water molecules. The gray data points represent what are evaluated from MD simulations, and the curves are the best fits to the Maxwell distribution functions (or the peak shifted ones). Notice that the temperatures are from the nonlinear fits to Maxwell velocity distribution functions and differ slightly from one case to another. Simulation parameters: 1 atm, with NPT ensemble.

TABLE 2: The Average Transport Velocities and the Peak Shifting Velocities of Hydronium and Water in the Hydrated PFSA Simulated at 300 K, 1 atm, and with Various Electric Fields (units: *E*, V/μm; v, m/s)

E	$\bar{v}_h$	$\bar{v}_w$	$v_{0,h}$	$v_{0,w}$
0	0.0	0.0	0.0	0.0
2	22.7	6.7	21.9	6.7
5	243.1	68.8	216.1	61.4
7	450.9	101.6	382.7	79.2
10	759.6	128.4	588.3	74.8

electrolyte membrane fuel cell is about 20 mV/μm, which is about 100 times smaller than the one used in our simulations. On the other hand, our electric field is still much lower than the one used by others (>100 V/μm).[30−35] One reason to avoid high electric field in experiment is the heat dissipation problem, the electric heat will cause the temperature increase, and thus denaturation of the biomolecules or even the fast evaporation of the water. If the heat dissipation problem could be solved in experiment, the electric field could be increased to obtain better separation efficiency. For example, if the heat dissipation in the microfluidic or the nanofluidic systems is much more efficient than that in the frequently used common laboratory equipment, the electric field could be significantly increased in these small systems. In MD simulations, the temperature can be maintained by removing heat from the system numerically via a procedure called the thermostat.[41,44] If the electric heat is too enormous in the case of extremely strong electric field, the temperature cannot be controlled even in MD simulations. For example, our simulations show that the system reaches more than 400 K at 5 V/μm with the Nosé−Hoover thermostat applied at every time steps. In Table 1, we list various temperatures evaluated from the velocity distribution functions of hydroniums and water molecules from MD simulations using the methods discussed in section 2.3. It could be seen that the temperatures are well maintained at about 300 K when there is no electric field applied. However, when the electric field increases to 2 V/μm, the temperature of hydronium increases to about 310 K and that of water increases to about 306 K. On the one hand, the increase in temperatures of hydronium is a direct result of the electric work that is constantly injected during each simulation step, while the applied thermostat cannot remove all the work as quickly as it is injected. On the other hand, the increase in the temperature of water is caused by the energy that is transferred from hydroniums to water molecules during their collision or by the drag of the associated hydroniums. The momentum is also transferred from hydroniums to water molecules during the collisions, and thus, the electroosmotic transport of water molecules occurs. By comparing the temperatures at various electric fields, the temperature increase at 2 V/μm is quite low, the temperatures will increase to well above the boiling point of water at 5, 7, or 10 V/μm. Another interesting phenomenon is the temperature differences in the direction of the applied electric field ($T_{||}$) and in directions perpendicular to the applied electric field ($T_{\perp}$), $T_{||}$ is 2.7 K higher than $T_{\perp}$ for hydronium, and $T_{||}$ is 0.8 K higher than $T_{\perp}$ for water. Since the temperature difference between hydronium and water is greater than that between different directions of the same component, we could deduce that the kinetic energy rearrangement between different directions is more efficient than that between different components. From these discussions, we can conclude that an electric field of 2 V/μm will not significantly disturb the motion of the hydroniums and water molecules in our MD simulations and it is suitable for the study of electroosmotic transport.

TABLE 3: The Average Transport Velocities, the Peak Shifting Velocities, and Electroosmotic Drag Coefficients Simulated with an Electric Field of 2 V/μm and at Various Temperatures (units: *T*, °C; *v*, m/s)

T	$\bar{v}_h$	$\bar{v}_w$	$v_{0,h}$	$v_{0,w}$	K^a_{drag}	K^0_{drag}
14.0	17.8	5.1	17.4	4.8	6.41	6.25
36.2	22.7	6.7	21.9	6.7	6.63	6.84
46.3	25.1	6.9	24.1	6.8	6.20	6.34
67.0	32.6	9.1	33.3	9.3	6.33	6.26
73.0	38.8	11.1	37.6	10.9	6.41	6.52
91.5	51.1	14.8	49.1	14.3	6.49	6.53

3.4. The Evaluation of the Average Transport Velocities and the Peak Shifting Velocities. From the velocity distribution functions, we calculate the average transport velocities of the hydroniums and the water molecules induced by the electric field using eqs 12A and 12B. From Table 2, it is shown that the average transport velocity of hydronium is 22.7 m/s at 2 V/μm. And at 5, 7, and 10 V/μm, the average transport velocities suddenly increase to 243.1, 450.9, and 759.6 m/s. The sudden increase in the average transport velocity between 2 and 5 V/μm reflects the fact that the hydroniums are pulled out of the hydrophilic subphase by the electric field or the hydroniums escape from the hydrophilic subphase because of the thermal motion caused by the accumulated electric heat. The average transport velocity of the water molecules is much smaller than that of the hydroniums (Table 2). Actually, the average transport velocities of the water molecule are only 30%, 28%, 23%, and 17% that of hydronium at 2, 5, 7, and 10 V/μm, respectively.

From Table 2, it could also be found that the average transport velocities and the peak shifting velocities show similar values when the electric field is weak. However, the difference between the average transport velocity and the peak shifting velocity increases as the electric field increases. This characteristic is caused by the fact that the attraction between the hydroniums and water molecules decreases as the electric field and the temperature increase; therefore, the momentum transfer efficiency between the hydroniums and water molecules decreases.

3.5. The Evaluation of Electroosmotic Drag Coefficient. Our simulations show that the microstructure of the hydrated PFSA is not significantly influenced by an electric field at 2 V/μm; however, significant changes are observed with an electric field at 5 V/μm or above. Furthermore, the velocity distribution function obeys the Maxwell distribution function or the peak-shifted Maxwell distribution function at an electric field of 2 V/μm or below, and at 5 V/μm or above, the velocity distribution functions do not obey the Maxwell distribution functions or the peak-shifted ones. Our simulations also show that temperatures of the simulation system could be maintained within about 10 K at 2 V/μm. From these results, we conclude that an electric field of 2 V/μm is suitable for the MD simulation study of electroosmotic drag of waters in the hydrated PFSA, since the microstructure of hydrated PFSA and the motion characteristics of the hydroniums and water molecules are not significantly disturbed and good statistical convergence could be obtained under this electric field. On the other hand, hydroniums will be pulled out of the hydrophilic subphase or escape the intermolecular attraction because of heat accumulation at 5 V/μm or above.

We evaluate the electroosmotic drag coefficient in hydrated PFSA under various temperatures with an electric field of 2 V/μm applied. Table 3 lists the average transport velocities and peak shifting velocities of the hydroniums and water molecules evaluated from MD simulations. It could be seen that the average transport velocities and the peak shifting velocities match each other very well. The electroosmotic drag coefficients K^a_{drag} calculated with eq 9 from the average transport velocities are also in good agreement with K^0_{drag} calculated from the peak shifting velocities (Table 3).

3.6. The Water Transport Mechanisms with an Electric Field Applied. The hydroniums transport in the direction of the electric field by the electric dragged, and a proton is carried by the transporting hydronium. This is the so-called vehicle mechanism.[45] On the other hand, the water molecules will not be directly dragged by the external electric field. However, momentum is transferred from the hydroniums to the water molecules during their collisions since hydronium has a net average transport velocity. This water transport mechanism depends on the momentum transfer during collision, and collision frequency increases with the temperature, thus the electroosmotic drag coefficient caused by collision also increases with temperature. This water transport mechanism is fully considered by our atomistic MD simulations.

Another water transport mechanism that is fully considered in our MD simulation is the associated transport. A hydronium is usually associated by a few water molecules via hydrogen bond. When the hydronium is accelerated, the associated water molecules are dragged by the hydronium. Since the association between hydroniums and water molecules breaks as the temperature increases, the electroosmotic coefficient caused by association with hydronium will decrease as the temperature increases. The water transport by associated hydroniums is implemented into our MD simulations via the force field model. The TIP3P model is a good model to count the association between hydroniums and water molecules.

The third water transport mechanism is a direct effect of the hopping mechanism of proton transport. This is an indirect acceleration of the neutral water molecule by the electric field. When a proton associated with a water molecule forms a hydronium, the hydronium is accelerated by the electric field. When the proton hops to the next water molecule, the first water molecule has been accelerated by the electric field during its association with the proton. However, the proton loses momentum because its newly associated water molecule has a lower momentum than the first water molecule. As the hopping process continues, momentum is exchanged between the hydroniums and the water molecules, thus more and more water molecules gain net transport momentum. In our MD simulations, both the proton hopping mechanism and the hopping-related water transport mechanism are not allowed due to the nondissociable force field used for the O−H bond. Since the hopping frequency increases with the temperature, the momentum exchange efficiency increases with the increase of temperature. Therefore, the hopping-related water transport increases with temperature.

Supposing that J_h(veh) is hydronium flow by the vehicle mechanism and J_p(hop) is proton flow by the hopping mechanism, and J_w(no hop) and J_w(hop) are water flows by the lack of hopping mechanism and by the exclusive hopping mechanism. The electroosmotic drag coefficient could be evaluated by,

$$K_{drag} = \frac{J_w(\text{no hop}) + J_h(\text{veh}) + J_w(\text{hop})}{J_h(\text{veh}) + J_p(\text{hop})} \qquad (15)$$

Although proton hopping is not allowed in our simulations, we can evaluate proton hopping by its relative contribution to the proton conductivity. The reported contribution to the proton conductivity from the vehicle mechanism is 22%,[46] thus the hopping flow is 3.54 times that of the vehicle flow. That is to say, $J_p(\text{hop}) = 3.54 J_h(\text{veh})$. However, we still do not know the

water flow by the hopping-related mechanism. If we suppose that the water flow by the hopping-related mechanism is zero, or $J_w(\text{hop}) = 0$, the electroosmotic drag coefficient calculated from eq 9 is overestimated, and the real electroosmotic drag coefficient will be only 0.22 of the calculated one. Our calculated electroosmotic drag coefficient is about 6.4 (Table 3); the real electroosmotic drag coefficient should be about 1.4. On the other hand, if we suppose that the water flow by the hopping-related mechanism equals the water flow without the hopping mechanism, or $J_w(\text{hop}) = J_w(\text{no hop}) + J_h(\text{veh})$, the real electroosmotic drag coefficient will be 0.44 of the calculated one. In our case, the electroosmotic drag coefficient should be about 2.8. Since it is unknown what percent of water is transported by the hopping-related mechanism, the accurate evaluation of electroosmotic drag coefficient is still impossible. Furthermore, the relative contributions from the vehicle mechanism or hopping mechanism to the proton transport are also variable depending on the hydration degree and morphology;[16] the accurate evaluation of the electroosmotic flow depends on the understanding of the proton conducting mechanism.

Our simulation results for the electroosmotic drag coefficient show very good correspondence with experimental values reported in the literatures. For example, Ise reported an electroosmotic drag coefficient of 2.6 at 300 K, 2.9 at 317 K, and 3.4 at 350 K in entirely hydrated Nafion 117 membrane (hydration degree of ~20) using electrophoresic nuclear magnetic resonance.[17,47] Ren et al. reported an electroosmotic drag coefficient of 1.9 at 15 °C and 5.1 at 130 °C in a direct methanol fuel cell.[48] Paddison et al. reported an electroosmotic drag coefficient of 1 for in water vapor equilibrated Nafion and 2−3 for in water immersed Nafion.[49]

From Table 3, it is shown that our simulations show no or very weak temperature dependence. This is also in accordance with some of the experimental measurements since some of the experimental works reported weak temperature dependence,[17,47] while others reported temperature dependence.[48]

4. Conclusions

A new atomistic MD simulation method for the study of electroosmotic drag based on the molecular velocity distribution functions in hydrate PFSA membrane has been developed. This method is superior to the direct evaluation of the average transport velocities of hydroniums and water molecules because much weaker electric field is required for the accurate evaluation of the average transport velocities, and thus the electric field applied during the MD simulation is weak enough not to perturb the microstructure of hydrated PFSA and the motion characteristics of hydroniums and water molecules.

It is also concluded that the velocity distribution functions of hydroniums and water molecules in the direction of the applied electric field obey the peak shifted Maxwell velocity distribution functions under weak electric field despite the great complexity of the hydrated PFSA structure and that the Maxwell velocity distribution functions are deduced from simple gaseous molecules. Two methods for the evaluation of electroosmotic drag coefficient, one from the average transport velocities and one from the peak shifting velocities, are equivalent and give similar results.

Three mechanisms for the water transport in hydrated PFSA are proposed: the associated mechanism, the collision mechanism, and the hopping-related mechanism. The MD simulation method that does not apply a dissociable O−H bond force field cannot be used for the evaluation of the hopping-related mechanism.

Our simulation also shows that the electroosmotic drag coefficient in hydrated PFSA has no or very weak temperature dependence.

Acknowledgment. This job is funded by the Department of Education of Shanghai and the Pujiang project of Shanghai Science & Technology Committee (No. 07PJ14044).

References and Notes

(1) Zhang, J.; Xie, Z.; Zhang, J.; Tang, Y.; Song, C.; Navessin, T.; Shi, Z.; Song, D.; Wang, H.; Wilkinson, D. P. High temperature PEM fuel cells. *J. Power Sources* **2006**, *160* (2), 872−891.

(2) Grant, P. M. Hydrogen lifts off-with a heavy load. *Nature* **2003**, *424* (6945), 129−130.

(3) Yan, L.; Balbuena, P. B.; Seminario, J. M. Perfluorobutane sulfonic acid hydration and Interactions with O_2 Adsorbed on Pt_3. *J. Phys. Chem. A* **2006**, *110* (13), 4574−4581.

(4) Seminario, J. M.; Agapito, L. A.; Yan, L.; Balbuena, P. B. Density functional theory study of adsorption of OOH on Pt-based bimetallic clusters alloyed with Cr, Co, and Ni. *Chem. Phys. Lett.* **2005**, *410* (4−6), 275−281.

(5) Stamenkovic, V. R.; Fowler, B.; Mun, B. S.; Wang, G.; Ross, P. N.; Lucas, C. A.; Markovic, N. M. Improved Oxygen Reduction Activity on $Pt_3Ni(111)$ via Increased Surface Site Availability. *Science* **2007**, *315* (5811), 493−497.

(6) Yang, C.; Costamagna, P.; Srinivasan, S.; Benziger, J.; Bocarsly, A. B. Approaches and technical challenges to high temperature operation of proton exchange membrane fuel cells. *J. Power Sources* **2001**, *103* (1), 1−9.

(7) Doyle, M.; Choi, S. K.; Proulx, G. High-temperature proton conducting membranes based on perfluorinated ionomer membrane-ionic liquid composites. *J. Electrochem. Soc.* **2000**, *147* (1), 34−37.

(8) Yan, L.; Zhu, S.; Ji, X.; Lu, W. Proton Hopping in Phosphoric Acid Solvated NAFION Membrane: A Molecular Simulation Study. *J. Phys. Chem. B* **2007**, *111* (23), 6357−6363.

(9) Buie, C. R.; Posner, J. D.; Fabian, T.; Cha, S.-W.; Kim, D.; Prinz, F. B.; Eaton, J. K.; Santiago, J. G. Water management in proton exchange membrane fuel cells using integrated electroosmotic pumping. *J. Power Sources* **2006**, *161* (1), 191−202.

(10) Okada, T.; Xie, G.; Meeg, M. Simulation for water management in membranes for polymer electrolyte fuel cells. *Electrochim. Acta* **1998**, *43* (14−15), 2141−2155.

(11) Wang, Z. H.; Wang, C. Y.; Chen, K. S. Two-phase flow and transport in the air cathode of proton exchange membrane fuel cells. *J. Power Sources* **2001**, *94* (1), 40−50.

(12) Ugur, P.; Chao-Yang, W. Two-Phase Modeling and Flooding Prediction of Polymer Electrolyte Fuel Cells. *J. Electrochem. Soc.* **2005**, *152* (2), A380−A390.

(13) Tuber, K.; Pocza, D.; Hebling, C. Visualization of water buildup in the cathode of a transparent PEM fuel cell. *J. Power Sources* **2003**, *124* (2), 403−414.

(14) Karimi, G.; Li, X. Electroosmotic flow through polymer electrolyte membranes in PEM fuel cells. *J. Power Sources* **2005**, *140* (1), 1−11.

(15) Pivovar, B. S. An overview of electro-osmosis in fuel cell polymer electrolytes. *Polymer* **2006**, *47* (11), 4194−4202.

(16) Kreuer; K.-D.; Paddison, S. J.; Spohr, E.; Schuster, M. Transport in Proton Conductors for Fuel-Cell Applications: Simulations, Elementary Reactions, and Phenomenology. *Chem. Rev.* **2004**, *104* (10), 4637−4678.

(17) Ise, M.; Kreuer, K. D.; Maier, J. Electroosmotic drag in polymer electrolyte membranes: an electrophoretic NMR study. *Solid State Ionics* **1999**, *125* (1−4), 213−223.

(18) Jinnouchi, R.; Yamada, H.; Morimoto, Y. "Measurement of electroosmotic drag coefficient of Nafion using a concentration cell", presented at 14th international conference on the properties of water and steam, Kyoto, 2004.

(19) Slater, G. W.; Desruisseaux, C.; Hubert, S. J.; Mercier, J.-F.; Labrie, J.; Boileau, J.; Tessier, F.; Pépin, M. P. Theory of DNA electrophoresis: A look at some current challenges. *Electrophoresis* **2000**, *21* (18), 3873−3887.

(20) Probstein, R. F. *Physicochemical Hydrodynamics*; Wiley: New York, 1994.

(21) Harrison, D. J.; Fluri, K.; Seiler, K.; Fan, Z.; Effenhauser, C. S.; Manz, A. Micromachining a Miniaturized Capillary Electrophoresis-Based Chemical Analysis System on a Chip. *Science* **1993**, *261* (5123), 895−897.

(22) Kuo, T. C.; Cannon, D. M.; Chen, Y.; Tulock, J. J.; Shannon, M. A.; Sweedler, J. V.; Bohn, P. W. Gateable Nanofluidic Interconnects for Multilayered Microfluidic Separation Systems. *Anal. Chem.* **2003**, *75* (8), 1861−1867.

(23) Helmholtz, H. Studieren uber electrische Grenzschichten. *Weid. Ann.* **1879**, *7*, 337−382.
(24) Lamb, H. *Philos. Mag.* **1888**, *5*, 52.
(25) Perrin, J. *J. Chim. Phys.* **1904**, *2*, 601.
(26) Smoluchowski, M. *Handbuck der Elektrizität und des Magnetismus*; Barth: Leipzig, 1914; Vol. 2.
(27) Breslau, B. R.; Miller, I. F. A hydrodynamic model for electroosmosis. *Ind. Eng. Chem. Fundam.* **1971**, *10* (4), 554−565.
(28) Schaetzel, P.; Nguyen, Q. T.; Riffault, B. Statistical mechanics of diffusion in polymers: Conductivity and electroosmosis in ion exchange membranes. *J. Membr. Sci.* **2004**, *240* (1−2), 25−35.
(29) Nilson, R. H.; Griffiths, S. K. Influence of atomistic physics on electro-osmotic flow: An analysis based on density functional theory. *J. Chem. Phys.* **2006**, *125* (16), 164510.
(30) Dzubiella, J.; Hansen, J. P. Electric-field-controlled water and ion permeation of a hydrophobic nanopore. *J. Chem. Phys.* **2005**, *122* (23), 234706.
(31) Dzubiella, J.; Allen, R. J.; Hansen, J. P. Electric field-controlled water permeation coupled to ion transport through a nanopore. *J. Chem. Phys.* **2004**, *120* (11), 5001−5004.
(32) Kim, D.; Darve, E. Molecular dynamics simulation of electro-osmotic flows in rough wall nanochannels. *Phys. Rev. E* **2006**, *73* (5), 051203.
(33) Freund, J. B. Electro-osmosis in a nanometer-scale channel studied by atomistic simulation. *J. Chem. Phys.* **2002**, *116* (5), 2194−2200.
(34) Crozier, P. S.; Rowley, R. L.; Holladay, N. B.; Henderson, D.; Busath, D. D. Molecular Dynamics Simulation of Continuous Current Flow through a Model Biological Membrane Channel. *Phys. Rev. Lett.* **2001**, *86* (11), 2467.
(35) Qiao, R.; Aluru, N. R. Charge Inversion and Flow Reversal in a Nanochannel Electro-osmotic Flow. *Phys. Rev. Lett.* **2004**, *92* (19), 198301.
(36) Jorgensen, W. L.; Chandrasekhar, J.; Madura, J. D.; Impey, R. W.; Klein, M. L. Comparison of simple potential functions for simulating liquid water. *J. Chem. Phys.* **1983**, *79* (2), 926−935.
(37) Neria, E.; Fischer, S.; Karplus, M. Simulation of activation free energies in molecular systems. *J. Chem. Phys.* **1996**, *105* (5), 1902−1921.
(38) Urata, S.; Irisawa, J.; Takada, A.; Shinoda, W.; Tsuzuki, S.; Mikami, M. Molecular Dynamics Simulation of Swollen Membrane of Perfluorinated Ionomer. *J. Phys. Chem. B* **2005**, *109* (9), 4269−4278.
(39) Smith, W.; Leslie, M.; Forester, T. R. *Computer code DL_POLY_2.14*: CCLRC, Daresbury Laboratory, Daresbury, England, 2003.
(40) Nosé, S. A molecular-dnamics method for simulations in the canonical ensemble. *Mol. Phys.* **1984**, *52* (2), 255−268.
(41) Nosé, S. A unified formulation of the constant temperature molecular dynamics methods. *J. Chem. Phys.* **1984**, *81* (1), 511−519.
(42) Verlet, L. Computer "Experiments" on Classical Fluids. I. Thermodynamical Properties of Lennard-Jones Molecules. *Phys. Rev.* **1967**, *159* (1), 98−103.
(43) Nandan, D.; Mohan, H.; Iyer, R. M. Methanol and water uptake, densities, equivalental volumes and thicknesses of several uni- and divalent ionic perfluorosulphonate exchange membranes (Nafion-117) and their methanol-water fractionation behaviour at 298 K. *J. Membr. Sci.* **1992**, *71* (1−2), 69−80.
(44) Hoover, W. G. Canonical dynamics: Equilibrium phase-space distributions. *Phys. Rev. A* **1985**, *31* (3), 1695−1697.
(45) Kreuer, K. D. On the complexity of proton conduction phenomena. *Solid State Ionics* **2000**, *136−137*, 149−160.
(46) Kreuer, K. D.; Rabenau, A.; Weppner, W. Vehicle mechanism; a new model for the interpretation of the conductivity of fast proton conductors. *Angew. Chem., Int. Ed. Engl.* **1982**, *21* (3), 208.
(47) Ise, M. Polymer-Elektrolyt-Membranen: Untersuchungen zur Mikrostruktur und zu den Transporteigenschaften für Protonen und Wasser, Max-Planck-Institut für Festkör-perforschung, Stuttgart, 2000.
(48) Ren, X.; Henderson, W.; Gottsfeld, S. Electro-osmotic drag of water in ionomeric membranes—New measurements employing a direct methanol fuel cell. *J. Electrochem. Soc.* **1997**, *144* (9), L267−L270.
(49) Paddison, S. J.; Paul, R.; Zawodzinski, T. A. Ion and water transport in a Nafion membrane pore: a statistical mechanical model with molecular structure, PV 98-27, The Electrochemical Society Proceedings Series, NJ, 1999, p 106.